Analysis of land use land cover change in Delhi, India over a period of 2000 to 2020

A Thesis submitted to the faculty of
San Francisco State University
In partial fulfillment of
the requirements for
the Degree

Master of Science

In

Geographic Information Science

by

Pravalika Ravula

San Francisco, California

August   2025

Certification of Approval

I certify that I have read Analysis of land use land cover change in Delhi, India over a period of 2000 to 2020 by Pravalika Ravula, and that in my opinion this work meets the criteria for approving a thesis submitted in partial fulfillment of the requirement for the degree Master of Science in Geographic Information Science at San Francisco State University.

Leonhard Blesius, Ph.D.
Professor

Jerry D Davis, Ph.D.
Professor

Abstract

This study examines the spatiotemporal dynamics of land use and land cover (LULC) in the city of Delhi, India, from 2000 to 2020. Multi-temporal satellite imagery from Landsat 7 (ETM+) for 2000 and Landsat 8 (OLI) for 2020 was used. ENVI's support vector machine (SVM) algorithm was employed for land use and land cover classification. Spectral indices such as NDVI, NDBI, NDWI, NDBSI, and a road index were generated using ArcGIS Pro and integrated to improve classification accuracy by helping differentiate vegetation, built-up areas, water bodies, bare soil, agriculture, fallow land, Ridge, and open land. ArcGIS Pro was further used for post-classification change detection and accuracy assessment. The overall classification accuracies for 2000 and 2020 were 80% and 83%, respectively, based on confusion matrix analysis, with corresponding Kappa coefficients of 0.75 and 0.79 indicating substantial agreement. The results showed a significant urban expansion on the outskirts of the city and an increase in built-up areas with vegetation in central Delhi. The study links these changes to infrastructure development, population growth, and policy interventions, emphasizing the importance of integrated land management in urban planning.

Acknowledgements

Table of Contents

List of Tables

List of Figures

List of Appendices

1 Introduction

Land use and land cover changes have emerged as major global concern due to their severe environmental and socio-economic impacts. Human activities like increase of agricultural land, deforestation, and urbanization are degrading natural landscapes and resulting in environmental degradation (King et al., 2023). These changes jeopardize biodiversity and have major impact on the local and global climatic conditions. The changes in land use and land cover (LULC), for instance, can modify the physical characteristics of the land surface and contribute to greenhouse gas emissions, which may impact local weather patterns and raise the risk of natural catastrophes (Bikis et al., 2025).

In this context, understanding and quantifying land use and land cover change has become a priority for researchers and policy makers. To study these changes, it is important to define the terms land use and land cover as these terms are often used interchangeably. The Food and Agriculture Organization (2024) define land cover as the observed physical and biological cover on earth's surface. On the other hand, land use refers to the arrangements, activities, and inputs applied by people to a land cover type to use or modify its surface.

LULC together provide a valuable framework to examine how human activity, societal needs, and development pressures are transforming the Earth's surface. This study aims to analyze the LULC changes in Delhi over a two-decade period using medium resolution Landsat satellite imagery. The findings will provide practical information for urban planners, environmental scientists, researchers, and decision-makers to build resilient and sustainable urban areas in metropolitan cities like Delhi.

2 Study area & Data

2.1 Study area:

The study area is the National Capital Territory (NCT) of Delhi, India, which holds the administrative status of a Union Territory with a special legislative assembly. Geographically, Delhi lies between 28°24'17'' and 28°53'00'' N latitudes, and 76°45'30'' E and 77°21'30'' E longitudes. To the north lie the Himalayan foothills, while the Aravalli ranges mark the southwestern edge of the territory (refer Figure 1). Delhi shares its eastern border with Uttar Pradesh and is surrounded on the north, west, and south by Haryana (Mohan et al., 2011). The Yamuna River, a tributary of the Ganges, flows through Delhi and provides the city with its primary water supply. In addition to its physical geography, Delhi holds historical, cultural, and political significance, functioning as a major hub for commerce, transportation, and governance in India (Ram et al., 2019).

Figure 1: Study area Delhi (left) and its location in India (right). Source: USGS Earth Explorer

Delhi experiences a humid subtropical climate, characterized by hot summers and dry winters (Kottek et al., 2006). The city sees significant temperature fluctuations throughout the year, ranging from around 5°C in winter to over 45°C in summer. The monsoon season, occurring between June and September, delivers the majority of the city's annual rainfall. These climatic variations strongly influence the LULC patterns, as well as the vegetation cycle in the region. In addition, rapid population growth has significantly impacted land use dynamics. Delhi's population has been steadily increasing since 1951.

2.2 Data:

For this study, the years 2000 and 2020 were selected to analyze land use and land cover changes in Delhi. Landsat ETM+ imagery from 2000 and Landsat OLI imagery from 2020 (refer Figure 2), both with a 30-meter spatial resolution, were obtained from the USGS Earth Explorer platform.

Table 1: Landsat ETM+ bands used in the study for the year 2000 (USGS, 2024)

Image	Scene ID	Layer	Band name	Wavelengths	Resolution / Acquisition date
1	LE71460402000074SGS00	1	Blue	0.45 - 0.52	30 / 2000/03/14
1	LE71460402000074SGS00	2	Green	0.52 - 0.60	30
1	LE71460402000074SGS00	3	Red	0.63 - 0.69	30
1	LE71460402000074SGS00	4	NIR	0.77 - 0.90	30
1	LE71460402000074SGS00	5	SWIR 1	1.55 - 1.75	30
1	LE71460402000074SGS00	6	Thermal	10.40 - 12.50	60 (resampled to 30)
1	LE71460402000074SGS00	7	SWIR 2	2.09 - 2.35	30
2	LE71470402000049SGS00	1	Blue	0.45 - 0.52	30 / 2000/02/18
2	LE71470402000049SGS00	2	Green	0.52 - 0.60	30
2	LE71470402000049SGS00	3	Red	0.63 - 0.69	30
2	LE71470402000049SGS00	4	NIR	0.77 - 0.90	30
2	LE71470402000049SGS00	5	SWIR 1	1.55 - 1.75	30
2	LE71470402000049SGS00	6	Thermal	10.40 - 12.50	60 (resampled to 30)
2	LE71470402000049SGS00	7	SWIR 2	2.09 - 2.35	30

For the year 2000, the data was acquired from Landsat ETM+ collection 2 level-2 from the dates 18 February 2000 and 14 March 2000 as shown in Table 1. For the year 2020, data was collected from Landsat OLI collection 2 level-2, with scenes dated 17 February 2020 and 17 February 2020. Table 2 provides the data acquition information for the year 2020.

Table 2: Landsat OLI bands used in the study for the year 2020 (USGS, 2024)

Image	Scene ID	Layer	Band name	Wavelengths	Resolution / Acquisition date
1	LC81460402020041LGN00	2	Blue	0.45 - 0.51	30 / 2020/02/10
1	LC81460402020041LGN00	3	Green	0.53 - 0.59	30
1	LC81460402020041LGN00	4	Red	0.64 - 0.67	30
1	LC81460402020041LGN00	5	NIR	0.85 - 0.88	30
1	LC81460402020041LGN00	6	SWIR 1	1.57 - 1.65	30
1	LC81460402020041LGN00	7	SWIR 2	2.11 – 2.29	30
1	LC81460402020041LGN00	10	TIRS 1	10.6 – 11.19	100 (resampled to 30)
2	LC81470402020048LGN00	2	Blue	0.45 - 0.51	30 / 2020/02/17
2	LC81470402020048LGN00	3	Green	0.53 - 0.59	30
2	LC81470402020048LGN00	4	Red	0.64 - 0.67	30
2	LC81470402020048LGN00	5	NIR	0.85 - 0.88	30
2	LC81470402020048LGN00	6	SWIR 1	1.57 - 1.65	30
2	LC81470402020048LGN00	7	SWIR 2	2.11 – 2.29	100 (resampled to 30)
2	LC81470402020048LGN00	10	TIRS 1	10.6 – 11.19	30
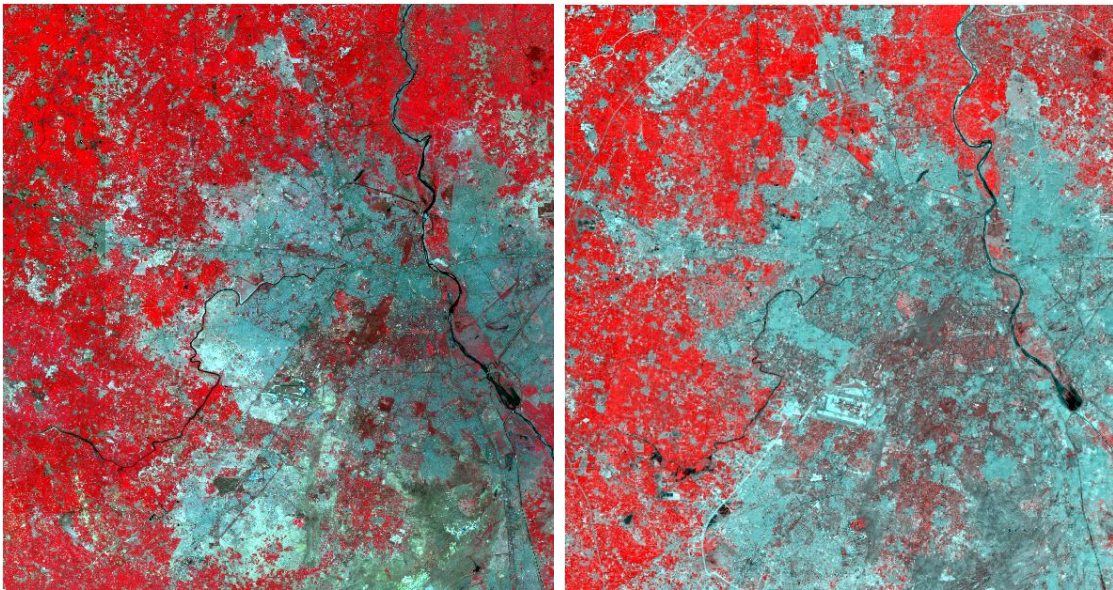
Figure 2: Landsat ETM+ (left) and Landsat OLI (right) data used for the classification for the years 2000 and 2020.

3 Methods

3.1 Image Pre-processing:

For this study, satellite images from both years were first layer-stacked and mosaicked using the Seamless Mosaic tool in ENVI 6.0 to create continuous and uniform coverage across the study region. The mosaicked images were then subset to the defined boundaries of the study area, Delhi.

3.2 Spectral Indices for classification accuracy:

To improve the accuracy of classification and change detection, five spectral indices were used: Normalized Difference Vegetation Index (NDVI), Normalized Difference Built-up Index (NDBI), Normalized Difference Water Index (NDWI), Normalized Difference Bare Soil Index (NDBSI), and a specialized Road Index (RI).

These indices are mathematical combinations of spectral bands that highlight specific land-cover features, thereby enhancing the separability of classes (e.g., vegetation, urban, water) in complex scenes (Tek Bahadur Kshetri, 2018). The values of these indices range from -1 to +1, where higher values represent the presence of the respective feature (e.g., vegetation in the context of NDVI), and lower or negative values indicate the presence of other features such as built-up areas or barren land.

3.2.1 NDVI:

NDVI helps in identifying green canopies and healthy vegetation by measuring the difference between near-infrared (NIR) and red light reflectance (Singh et al., 2022). In the NDVI maps (Figure 5), higher index values representing dense vegetation, such as tree cover,

parks, and agricultural land, are shown in green shades. Moderate values appear in yellow to light orange, typically indicating sparse or stressed vegetation. Lower values, corresponding to built-up areas, barren land, or water bodies, are shown in red shades. These maps were used to select training samples for vegetation and agricultural land classes. Values close to 0 typically indicate barren or sparsely vegetated areas, while negative values represent features such as water bodies and impervious surfaces.

$$NDVI = \frac{NIR - RED}{NIR + RED}$$

3.2.2 NDBI:

NDBI is used to identify urban or built-up areas. It is calculated using the short-wave infrared (SWIR-1) and near-infrared (NIR) bands. Materials such as concrete and asphalt reflect more strongly in the SWIR region compared to vegetation, which results in high NDBI values for built-up surfaces (Tek Bahadur Kshetri, 2018). In contrast, vegetation and water bodies tend to produce low or negative NDBI values.

$$NDBI = \frac{SWIR - NIR}{SWIR + NIR}$$

3.2.3 NDWI:

NDWI highlights water features such as rivers, lakes, and ponds by comparing green light reflectance to that of near-infrared (NIR). Visible green light enhances water reflectance, while NIR enhances the reflectance of vegetation and soil. As a result, water pixels appear with

high NDWI values, whereas built-up areas, soil, and vegetation show low values. This index is particularly useful for monitoring the Yamuna River in Delhi and detecting changes in the extent of surface water bodies.

$$NDWI = \frac{Green - NIR}{Green + NIR}$$

3.2.4 NDBSI:

NDBSI was computed to differentiate built-up areas from dry, bare soils. This index was recently developed to emphasize surface dryness and detect bare soil conditions (Liu et al., 2022). Positive NDBSI values indicate dry and non-vegetated surfaces, which in this study are represented by brown tones on the NDBSI maps (Kafy et al., 2020). In this study, the index was used to identify training samples for the classes open land, fallow land, and bare soil.

$$NDBSI = \frac{(RED + SWIR) - (NIR + BLUE)}{(RED+SWIR) + (NIR + BLUE)}$$

3.2.5 Road Index:

To improve the detection of linear infrastructural features during classification, the Road Index (RI) was used as an auxiliary indicator to identify built-up areas with road-like spectral behavior. Originally applied by Ahmed et al. (2022), this index emphasizes asphalt roads by combining bands from the visible, NIR, and SWIR regions of multispectral imagery. In this study, RI was not used to classify roads as a standalone land use class, but rather to support accurate detection of built-up areas by highlighting road networks. In the generated RI maps, higher index values corresponding to roads, highways, and railways are represented in red shades, while lower values corresponding to vegetation or non-linear surfaces appear in green. This contrast helped

prevent the misclassification of roads as bare soil or open land during the training sample collection.

$$RI = 1 - \frac{3 * BLUE}{BLUE + NIR + SWIR}$$

3.3. Classification methodology:

Supervised classification was carried out to generate LULC maps using the Support Vector Machine (SVM) algorithm in ENVI 6.0. SVM is a non-parametric machine learning classifier known for its high accuracy in remote sensing applications and its ability to generalize well from limited training samples (Mountrakis et al., 2011). Comparative studies have shown that SVM often outperforms traditional classifiers such as Maximum Likelihood Classifier (MLC) and Neural Networks (NN) (Pal & Mather, 2005). Its use of margin maximization and kernel functions enables effective class separation, even when the data is not linearly separable.

Table 3: Land use land cover classes

S. No.	Class Name	Description
1	Open land	Refers to unused spaces with no vegetation or built-up features.
2	Agriculture	Lands that are currently being used for farming and are characterized by field patters
3	Fallow land	Previously cultivated land left temporarily uncultivated.
4	Vegetation	Land with natural tree-cover such as forests.
5	Bare soil	Exposed soil surface along the riverbed and adjacent floodplain zone.
6	Ridge	The elevated rocky terrain, which is the extension of Aravalli hills, having sparse to moderate tree cover.
7	Built-up with vegetation	Built-up areas with visible tree-cover such as residential areas with urban green spaces.
8	Built-up without vegetation	Densely built-up areas with less or no vegetation and are dominated by imperious materials like concrete.
9	Water	Natural or human made water bodies like Yamuna River, lakes, ponds etc.

Regions of Interest (ROIs) were sampled for each land cover class based on spectral indices, spectral signatures, and visual interpretation of the satellite imagery. A total of nine land use and land cover classes were defined for analysis of the study area. Table 3 provides a description of each class. These classes represent the major thematic land cover categories in Delhi and were selected to be mutually exclusive and representative of the region's primary land types.

For the classification, the SVM classifier was applied using trained ROIs for each land cover class, with a radial basis function kernel and a one-against-one multi-class strategy as the default setting. The SVM algorithm labeled each pixel in the satellite images based on learned class boundaries in feature space, generating a thematic land cover map for each year. Post-classification smoothing and aggregation tools were used to reduce speckle noise and eliminate small fragmented regions.

The classification results for 2000 and 2020 were validated through an accuracy assessment using a confusion matrix (also known as an error matrix) in ArcGIS Pro 3.3. A confusion matrix is a widely used method for evaluating thematic classification accuracy (Congalton, 1991). For each year, over 500 stratified random sample points (Figure 3) were selected. These points were then cross-validated with Google Earth Pro's historical imagery for the year 2000 (approximately 15–30 m resolution) and current imagery for 2020 (approximately 0.5–5 m resolution) to generate the confusion matrix.

User's Accuracy (UA), Producer's Accuracy (PA), Kappa coefficient (κ), and Overall Accuracy (OA) were derived from the matrix. Overall Accuracy reflects the proportion of correctly classified pixels across all classes. Producer's Accuracy, also known as recall,

measures the likelihood that a reference sample of a certain class is correctly identified on the

classified map (Story & Congalton, 1986). On the other hand, User's Accuracy estimates the

probability that a pixel labeled as a given class on the map actually belongs to that class on the

ground, thereby accounting for commission errors (Story & Congalton, 1986).

Together with the Kappa coefficient, these accuracy metrics are commonly used by

researchers to validate classification results (Islami et al., 2022). For land use and land cover

classifications, an Overall Accuracy above 70% is generally considered acceptable (Islami et al.,

2022). By applying the confusion matrix approach, this study ensured a standardized and

quantitative validation of the classification results for both 2000 and 2020.
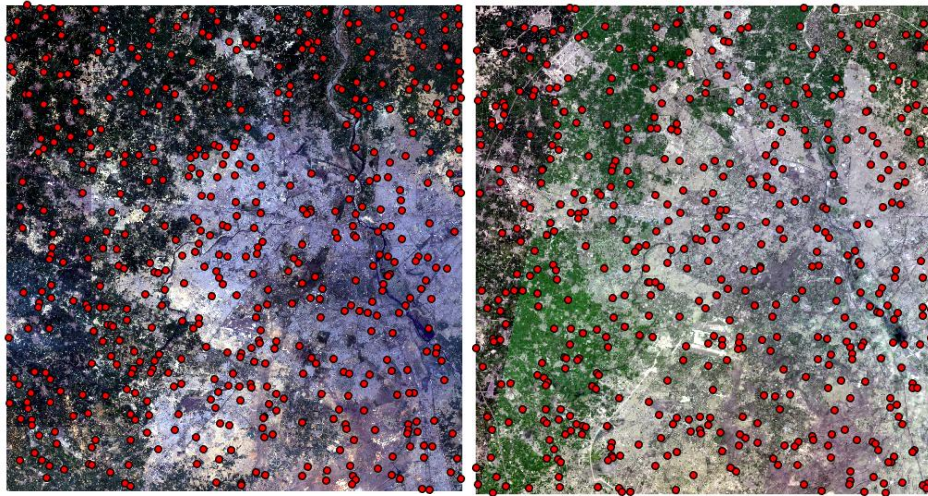
Figure 3: Strafified random accuracy assessment points for the year 2000 (left) and 2020 (right).

Post-classification comparison was conducted to generate a change detection map and

analyze LULC changes between 2000 and 2020 using ArcGIS Pro 3.3. The classified maps were

first reclassified to ensure consistent class definitions across both years and were then converted

into vector format to enable spatial overlay and analysis.
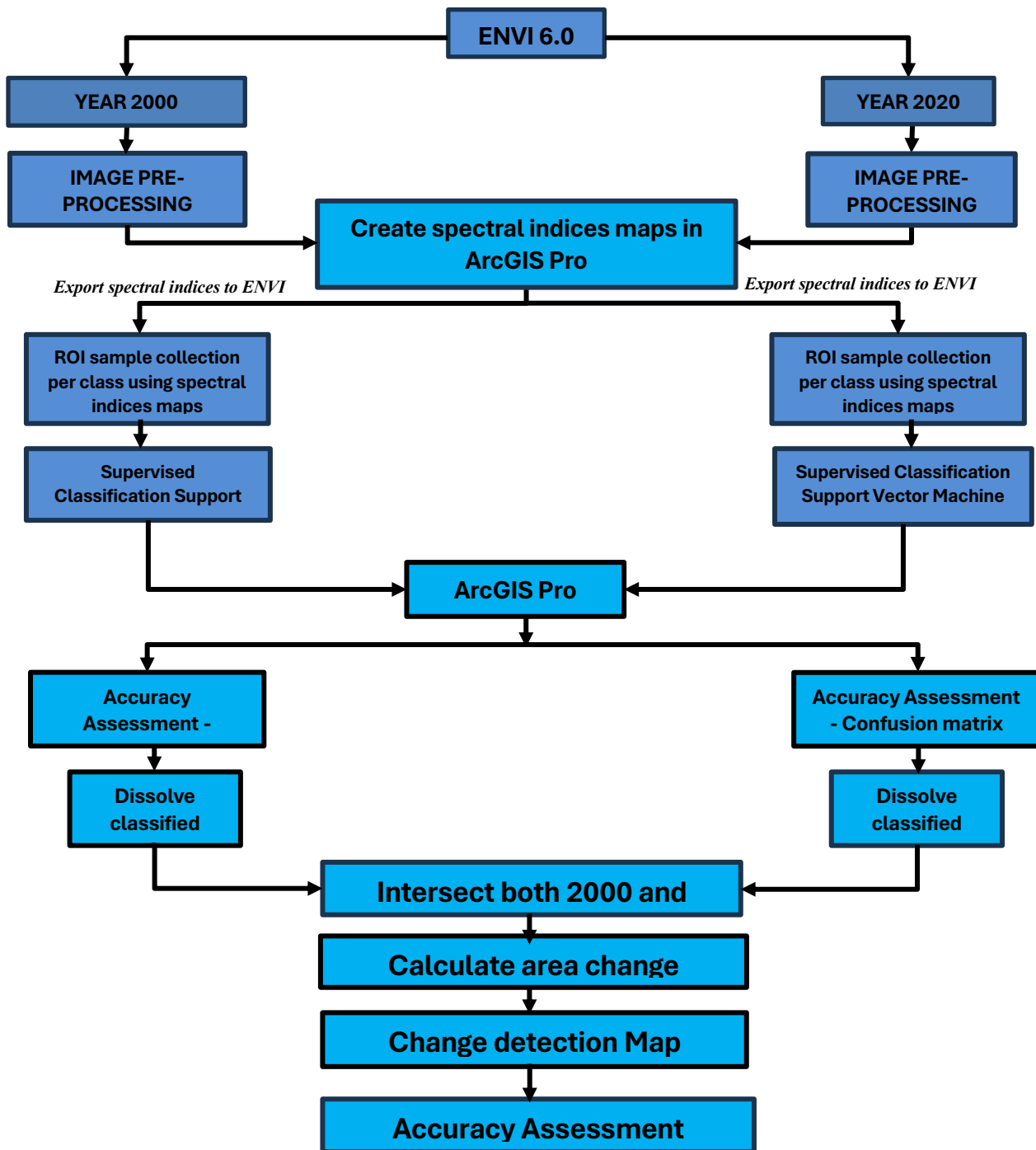
Figure 4: *Figure illutrates the step-by-step workflow followed in the study to generate the land use land cover maps and to perform change detection analysis for the years 2000 and 2020.*

Land cover changes were derived by intersecting the two vectorized maps. The area of each class was calculated to quantify the spatial extent of change (Li et al., 2023). This post-classification comparison method is widely used in change detection studies, as it provides detailed "from-to" transitions between land cover types and helps reduce discrepancies caused by atmospheric conditions or sensor differences (Li et al., 2023). Areas that experienced a land cover transition between 2000 and 2020 were categorized into nine change classes, while areas that remained unchanged were classified into nine stability classes. Based on these 18 categories, a comprehensive change detection map was produced and validated using the confusion matrix.

4. Results

4.1: Spectral Indices

Using five spectral indices; NDVI, NDBI, NDWI, NDBSI, and road index significantly improved both the accuracy of supervised SVM classification and the understanding of LULC dynamics. High-value pixels in each index map served as valid training examples for the respective classes, increasing separability and lowering misclassification. The comprehensive examination of Delhi's changing environment using these indicators was extremely useful in determining urban expansion and ecological alterations throughout time.

The NDVI results (Figure 5) reveal clear spatial changes in vegetation distribution between 2000 and 2020. In 2000, higher NDVI values (green shades) were concentrated along the Yamuna River, in agricultural zones, and on the city's periphery, while central areas showed lower values due to dense urbanization. By 2020, vegetation increased in certain northern and river-adjacent areas, but substantial green cover loss occurred in expanding built-up zones,
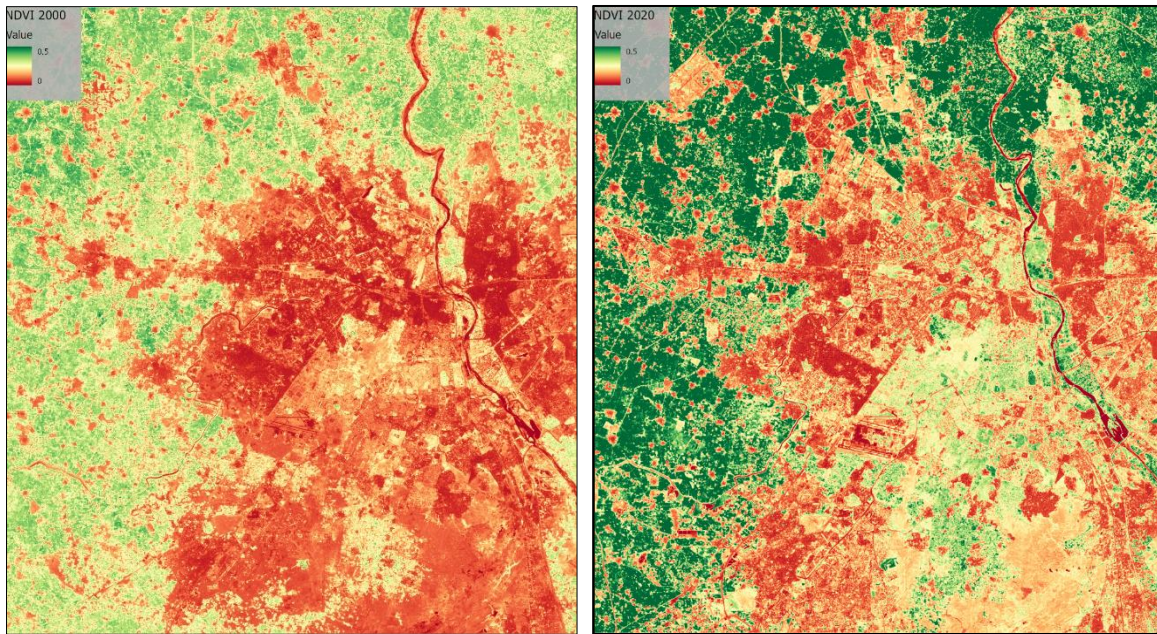
Figure 5: *NDVI results for the year 2000 (left) and 2020 (right) show index values ranging from 0 to 0.5. These maps help identify tree covers, parks and agricultural land, revealing vegetation changes over time.*

particularly in central and southwestern Delhi. These changes reflect both urban growth pressures and targeted greening efforts such as park restoration and plantation drives.

Urban expansion was most clearly indicated by the Normalized Difference Built-up Index (NDBI), where high positive values (red shades) mark dense built-up areas, and negative values (blue shades) represent water bodies or dense vegetation. Light orange to beige tones indicate moderately built-up or mixed land cover.

From 2000 to 2020, urban reflectance patterns intensified significantly, particularly in central, western, and southern Delhi. While some confusion occurred between the Ridge area and open terrain, the NDBI allowed for a more precise demarcation of urban footprints and helped identify built-up regions containing small vegetation patches (Figure 6). These observations align with Sharma and Joshi (2016), who reported significant built-up growth across Delhi-NCR from 1998 to 2011, largely at the expense of agricultural land.
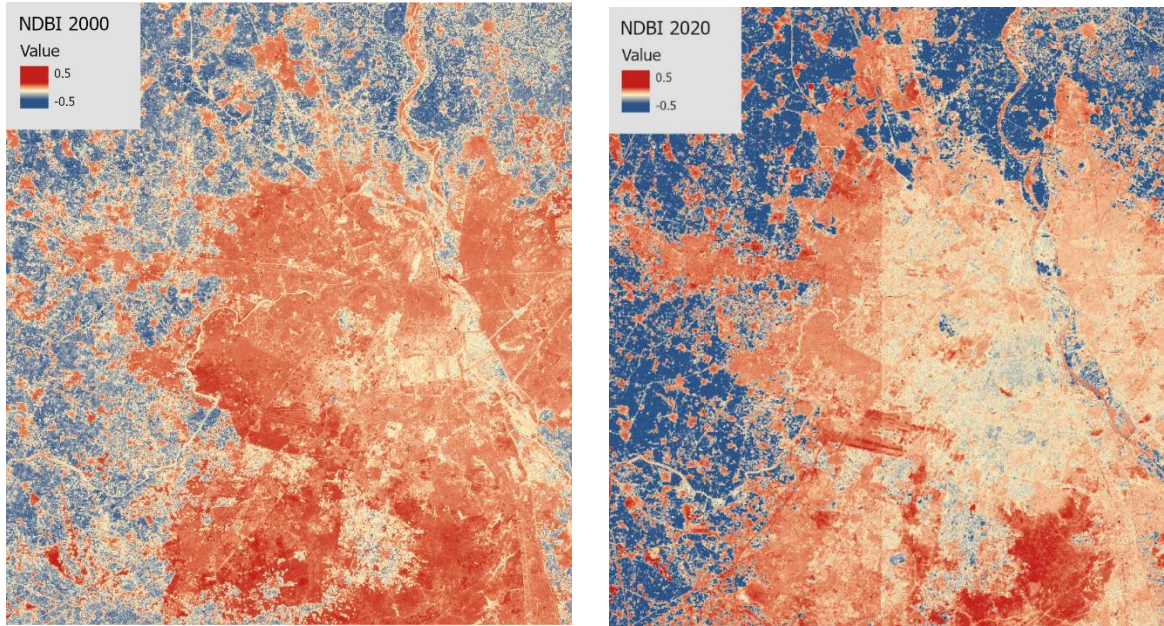
Figure 6: *NDBI maps for 2000 (left) and 2020 (right) showing built-up areas (red) and vegetation/water (blue), highlighting significant urban expansion in Delhi. Values range from –0.5 to 0.5.*
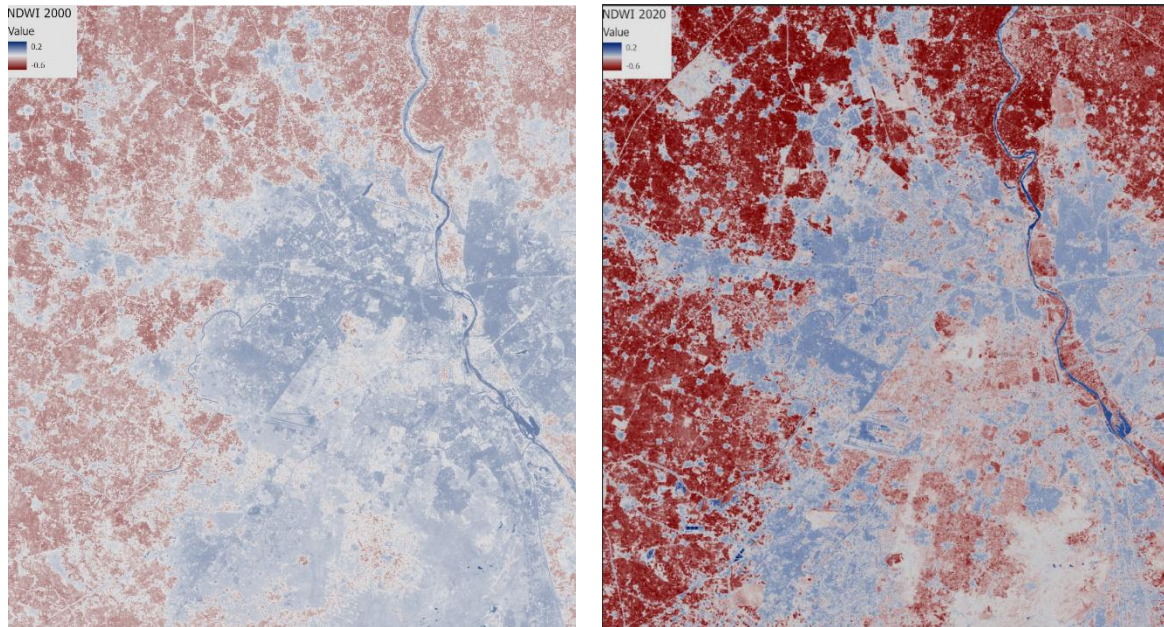
Figure 7: *Normalized Difference Water Index (NDWI) results for the year 2000 (left) and 2020 (right). Values range from –0.6 to 0.2, with higher positive values (blue) indicating water bodies and negative values (brown) representing non-water features such as built-up and vegetation areas.*

NDWI analysis found reasonably stable water bodies across time, with the Yamuna River and adjacent floodplains sustaining moderate to high index values in both years. The 2020 results were particularly obvious because of Landsat 8's increased radiometric sensitivity. Despite slight misunderstanding in wet vegetation regions, NDWI successfully caught main hydrological characteristics and aided in the interpretation of restored water zones (Figure 7). These findings represent continuous water restoration measures that helped to preserve aquatic regions around the city.
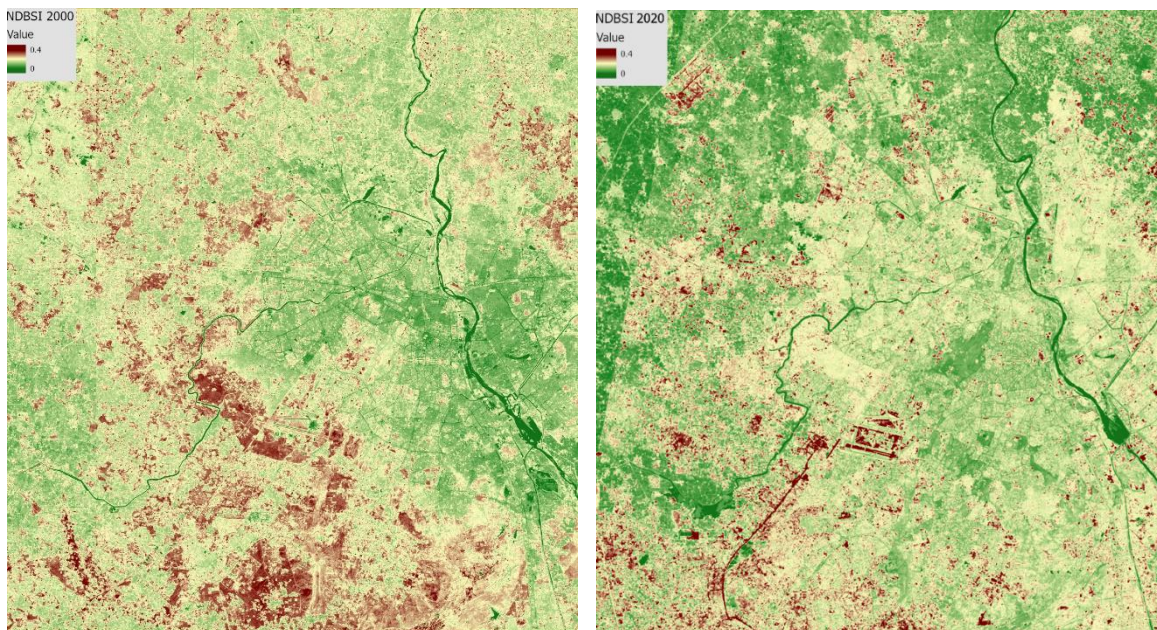
Figure 8: NDBSI results for the year 2000 (left) and 2020 (right) show index values ranging from -0.206 to 0.600 and -0.358 to 0.631 respectively. These maps help identify bare dry soil and open land.

The Normalized Difference Bareness Soil Index (NDBSI) was effective in detecting non-vegetated surfaces such as bare soil, fallow agricultural fields, and early-stage construction zones (Figure 8). Higher positive values (brown shades) correspond to bare or sparsely vegetated land, light yellow–beige tones indicate moderately dry or transitional areas, while negative values

(green shades) represent vegetated surfaces. Between 2000 and 2020, brown-shaded zones became more prominent in the southern and peripheral regions of Delhi, suggesting land clearing, soil exposure, and construction activity linked to urban expansion. Although the index sometimes overestimated bare soil in fallow farmland, it provided a consistent indicator of surface dryness and open land distribution.

The road index (RI) results (Figure 9) effectively highlight linear infrastructure such as roads, highways, railways, and bridges, which appear in red shades representing higher RI values. In contrast, vegetated areas appear green, allowing clear visual separation between built infrastructure and natural land cover. Between 2000 and 2020, there is a visible increase in red-toned linear features, indicating significant road network expansion, particularly toward the western, southern, and peripheral regions of Delhi.
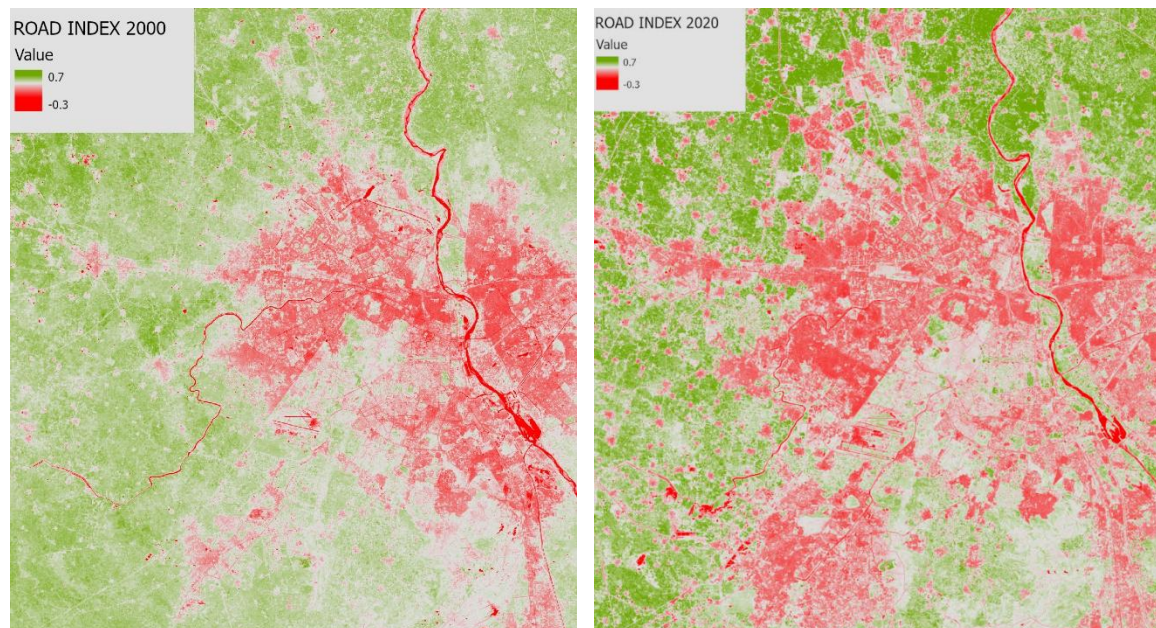
Figure 9: Road Index maps for 2000 (left) and 2020 (right), with values ranging from –0.3 (green, non-road areas) to 0.7 (red, road and built-up areas).

The 2020 map also shows enhanced connectivity along major corridors and ring roads, reflecting the city's rapid infrastructural growth. The RI also helps reduce misclassification of roads as bare soil, which is especially important in peri-urban and arid zones. These spatial patterns align with findings by Faizan (2022), who reported substantial transport corridor development in Delhi over the last two decades.
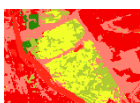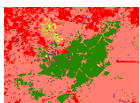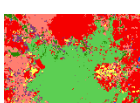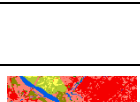
4.2: Classification results:

The supervised Support Vector Machine classifier successfully distinguished all nine land use and land cover classes with minimal confusion. As shown in Figure 10, Ridge areas, represented in light green, occupied a larger spatial extent in 2000 compared to 2020. Vegetation, shown in dark green, appears in scattered patches throughout the city. Open land, displayed in purple, is prominent in the year 2000, particularly in the Ridge extension and southeastern zones of Delhi.

Built-up without vegetation, shown in red, dominate the city landscape in 2000 but are largely replaced by built-up with vegetation (coral-pink) by 2020, indicating a shift toward greener urban zones. Bare soil is concentrated along the Yamuna River, while agricultural (chartreuse color) and fallow lands (canary yellow) are primarily located on the city's outskirts, with limited patches within the urban boundary.

The classification results also reveal a noticeable reduction in water bodies between 2000 and 2020, particularly along smaller tributaries and urban reservoirs. Expansion of built-up areas into former agricultural and open lands reflects the rapid pace of urbanization in the NCT of Delhi. These spatial transformations highlight the combined influence of population growth, infrastructure development, and changing land management practices over the past two decades.

Table 4: Areas covered by each land use land cover class

Land use land cover classes	Land use land cover class symbology	Area covered in the year 2000 (sq.km)	Area covered in the year 2020 (sq.km)	Absolute Change (sq.km)	Percentage of Change (relative to the year 2000)
Open land		100.1	47.2	-52.9	-52.9%
Agricultural land		931.7	833.5	-98.2	-10.5%
Fallow land		189.9	144.3	-45.6	-24%
Vegetation		61.1	70.5	+9.4	+15.4%
Bare soil		30	25.8	-4.3	-14.2%
Ridge		130	100.2	-29.8	-22.9%
Built-up with vegetation		365.9	672.9	+307	+83.9%
Built-up without vegetation		904.7	810.0	-94.7	-10.5%
Total built-up area		**1270.6**	**1482.9**	**+212.3**	**+16.7%**
Water		21.8	30.9	+9.1	+41.65%
Total area		**2735.2**	**2735.2**		
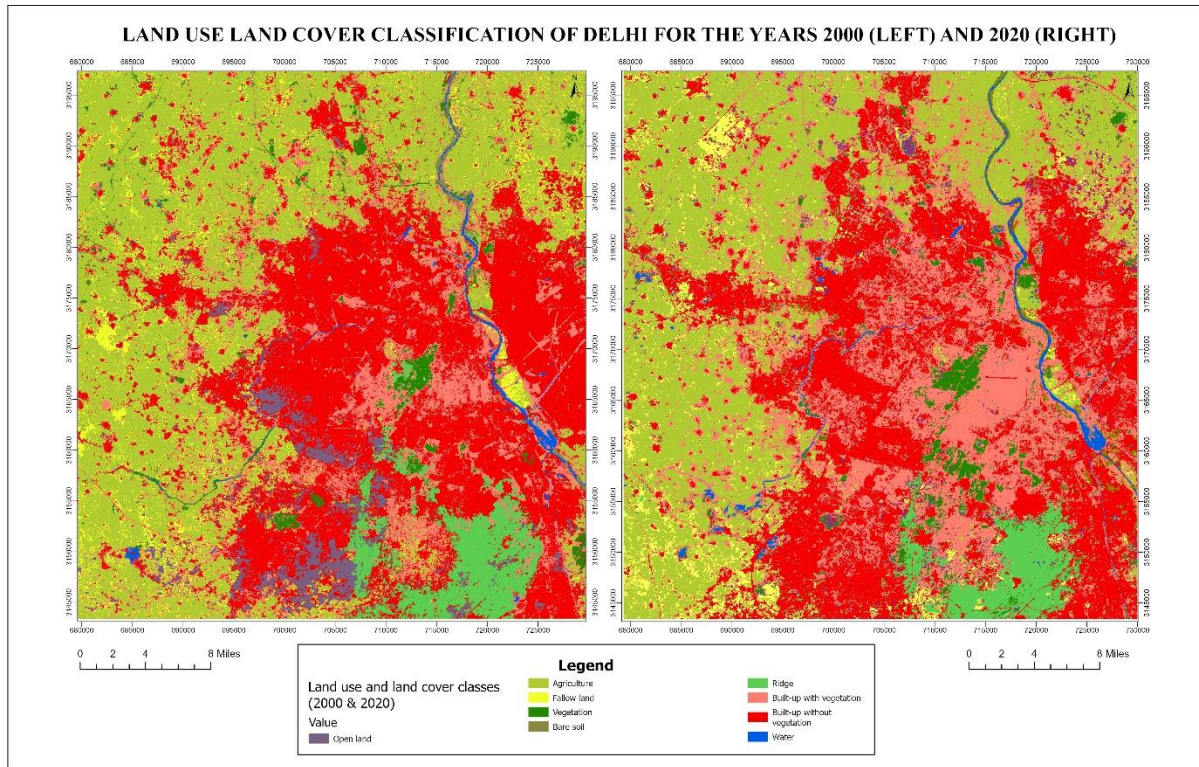
Figure 10: *Land use and land cover classification maps for the years 2000 (left) and 2020 (right) showing spatial distribution of nine classes including open land, agriculture, fallow land, vegeattion, bare soil, Ridge, built-up with vegetation, built-up without vegetation and water bodies. These maps highlight the urban expansion and land transition across Delhi over the two decade period.*

4.3: Land use land cover changes from 2000 to 2020

The analysis of Delhi's land use and land cover for the two decade period shows significant changes across each category. Table 4 above summarizes the changes in the area for each land use land cover class based on the classification maps.

Open land: Reduced from 100.1 km^2 in 2000 to 47.2 km^2 in 2020. This shows almost 53% of decrease in open land during the study period. Most of the open land has been used for built-up areas by 2020.

Agricultural land: Decreased from 931.7 km^2 to 833.5 km^2 representing an approximate 10.5% decline. Like open land most of the agricultural land was converted into urban expansion.

Fallow land: Declined from 189.9 km^2 to 144.3 km^2 with a 24% decrease. Many areas that remained uncultivated in 2000 were either cultivated or developed by 2020.

Vegetation: Increased from 61.1 km^2 to 70.5 km^2 reflecting a 15% increase. This includes the dense vegetation in the study area.

Bare soil: Decreased from 30 km^2 to 25 km^2 showing a 14% decrease.

Ridge: A Decline from 130 km^2 to 100.2 km^2 amounting to a 23% decrease. Despite the protected status of Delhi's Ridge, there is a reduction due to the construction of new settlements and expansion of the urban area.

Built-up with vegetation: This land use class expanded from 365.9 km^2 to 672.9 km^2 with 84% surge in the Built-up areas with tree cover which include urban green spaces.

Built-up without vegetation: Decreased from 904.7 km^2 to 810 km^2 wiith 10.5% decrease. This may be due to an increase in built-up with vegetation. However, the total built-up area still expanded from 1270.6 km^2 to 1482.9 km^2 reflecting a rise of almost 50% of the total study area by the year 2020.

Water: Increased from 21 km^2 to 30.9 km^2 with a 42% rise. Despite the results, the quality of water bodies in Delhi especially River Yamuna had been deteriorated over the years due to the release of industrial chemicals resulting in water pollution and need of attention.

The results clearly indicate that overall built-up area has drastically increased while most of the other LULC classes have decreased. In the year 2000, agriculture was dominant land use followed by built-up without vegetation. By 2020, most of the agriculture was converted into built-up areas resulting in decline in agriculture.

The decline in open land suggests that by 2020, very little land remained undeveloped or unused. The rise in the built-up with vegetation class indicates that many newly developed or modified urban areas now support tree cover through the expansion of city parks, rooftop plantations, roadside greenery, and other green infrastructure. In contrast, in 2000, the city contained only a limited extent of built-up areas with vegetation. The study's quantitative findings align with both the magnitude and direction of land use transitions reported in previous geospatial studies of Delhi's urban landscape (Mohan et al., 2011).

According to the classification maps, the spatial distribution of land use and land cover changes has been especially prominent along the city's peripheries, often at the expense of agricultural land (Figure 12). This shows that regions such as Northwest Delhi (e.g., Narela and Bawana), West and Southwest Delhi (e.g., Najafgarh), and the eastern areas across the Yamuna River (including parts of Shahdara and toward Noida) have undergone significant transformation, with a large number of villages and agricultural lands being urbanized into residential neighborhoods, infrastructure corridors, industrial zones, and commercial centers (Singh et al., 2023).

The tones of red showing urban land cover reflects the suburbanization in the 2020 classification map (see figure 10). In contrast, the same regions in the 2000 classification map show a patchwork of agricultural fields. Previously open and fallow lands are now being progressively infilled and developed at higher densities. Particularly on the outskirts of the city, scattered open lands visible in 2000 had largely disappeared by 2020. Approximately 53% of the lost open land area was converted into built-up land in some form (Figure 11). Similarly, many

fallow land areas present in 2000 have since been reclaimed for agricultural use or absorbed into expanding urban development.

Despite these changes, the increase in vegetation cover by 2020 is noticeable in central part of Delhi and near the area of Vasant Kunj, Malviya Nagar and Saket areas. This may be due to some part of Ridge in the southern part of the city got correctly classified in 2000 map while in 2020 it was classified as vegetation. This can be due to the tree cover of the Ridge might have been denser in 2020 than in 2000. Delhi's Ridge is known as the "green lungs" of the city and has seen a noticeable contraction by 2020. The vegetated area of the Ridge is experiencing encroachment, commercialization, construction of villages and unauthorized farmhouses despite legal protections and court orders. This led to the decrease in tree cover of southern Ridge area (Agarwal, 2025).

Water bodies showed a slight increase in spatial extent by 2020. This may be attributed to higher seasonal rainfall or the implementation of floodplain restoration efforts, such as the Najafgarh Jheel Restoration Plan and the Yamuna River Rejuvenation Project. The 2020 classification map displays a broader extent of the Yamuna River channel compared to 2000. In addition, several artificial lakes and ponds have been established through water harvesting initiatives in public parks and urban green spaces.

The Najafgarh Jheel area, located along the western boundary of Delhi, has historically shrunk from over 225 km² a century ago to just a few square kilometers in recent decades (GKToday, 2022). Although minor misclassifications may be present in the classified map, satellite data indicates a modest re-expansion of water coverage in this region by 2020. Similarly,

the observed decline in bare soil along the Yamuna River may be the result of river widening, sediment coverage, or classification overlap between water and exposed soil.

Overall, spatial trends show a concentric expansion of built-up areas between 2000 and 2020 at the cost of agricultural land, fallow, and open land. By 2020 most of the non-built-up areas remain largely in protected or low-lying areas like the Ridge and Yamuna floodplain.
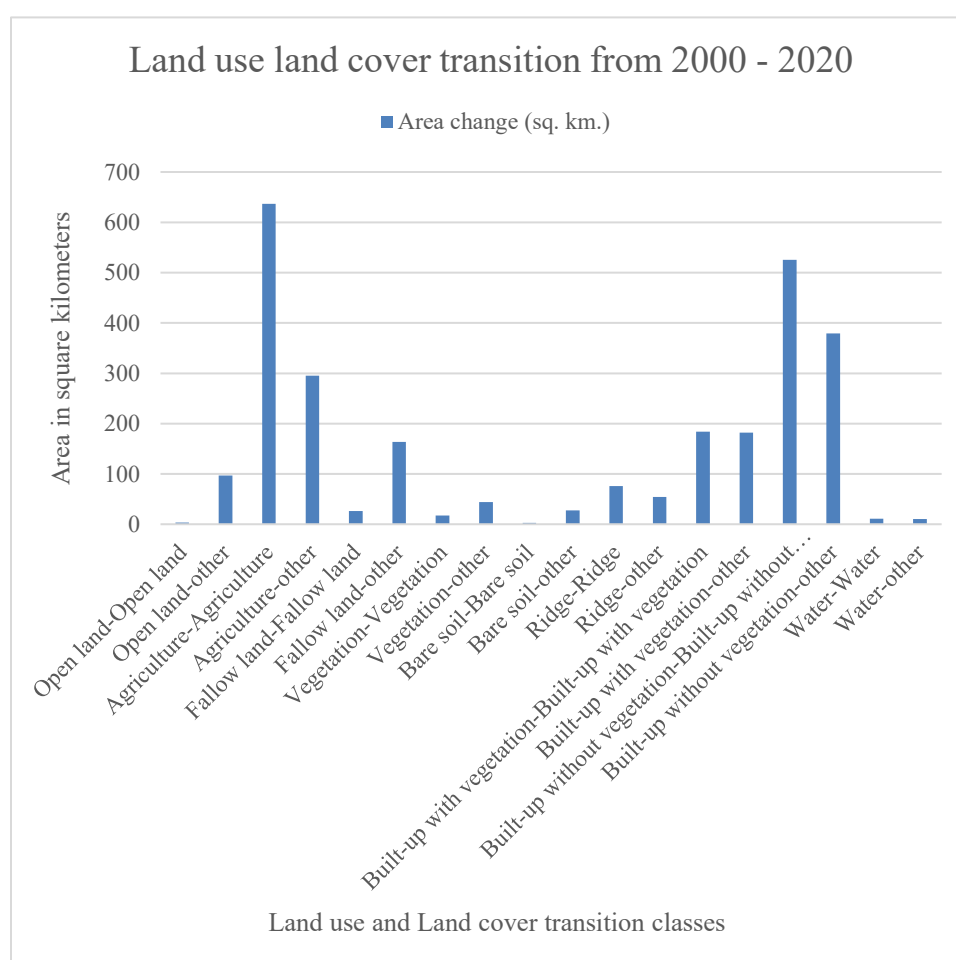
Figure 11: *The bar graph shows the land use land cover transition from 2000 to 2020. It compares the area (in sq.km) of each class across the two years. The graph highlights a notable decrease in open land, agricultural land, fallow land, while built-up areas increased reflecting urban expansion.*
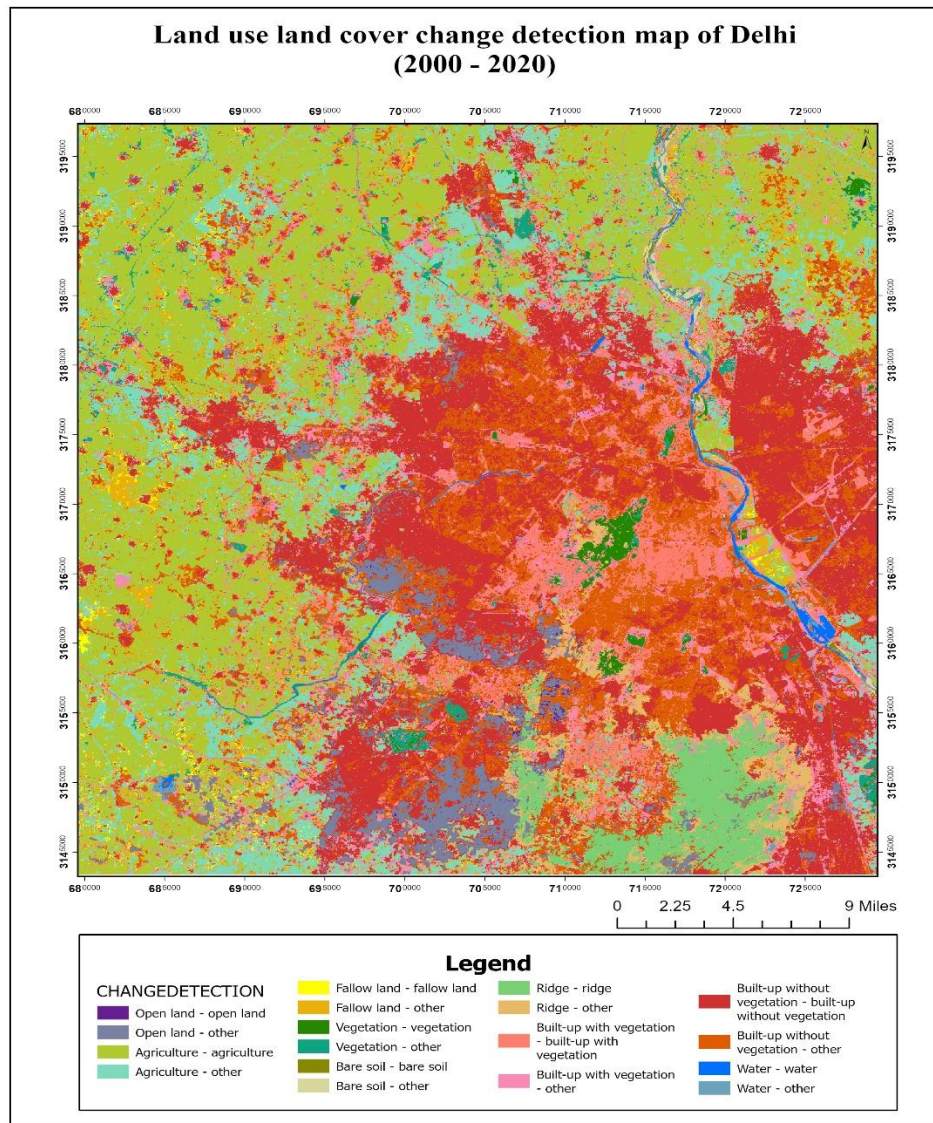
Figure 12: *Illustration of the land use land cover change detection map of Delhi from 2000 to 2020, visualizing the spatial shifts in land categories*

4.4 Accuracy Assessment:

For the year 2000, the land use and land cover classification achieved an overall accuracy of 80.04% and a Kappa coefficient of 0.749 (Table 7). Agricultural land, open land, and water emerged as the most reliable classes. Open land recorded a perfect User's Accuracy (UA) of 100% and a Producer's Accuracy (PA) of 52.38%, indicating that while all pixels classified as

open land were correct, nearly half of the actual open land pixels were omitted (Table 5).

Agricultural land performed strongly, with PA of 90% and UA of 98.08%, reflecting minimal

misclassification.

Built-up classes showed moderate to high performance: Built-up with vegetation

achieved PA of 81.72% and UA of 75.25%, while Built-up without vegetation attained PA of

92.63% and UA of 69.84%. Some misclassification occurred between these built-up types, ridge

areas, and open land. Vegetation displayed a high UA of 90.91% but a lower PA of 62.5%,

suggesting omission errors. Ridge areas had balanced but modest accuracy (PA 57.69%, UA

60%). Fallow land recorded PA of 60.78% and UA of 67.39%. Bare soil had the lowest accuracy

(PA 25%, UA 10%), largely due to spectral confusion with open land and built-up areas,

compounded by limited training samples. Water achieved 100% accuracy in both UA and PA.

For the year 2020, classification accuracy improved overall, reaching 83.04% overall

accuracy with a Kappa coefficient of 0.787 (Table 6). Most classes showed gains compared to

2000. Built-up without vegetation retained a high PA (92.38%) and improved UA to 76.96%.

Built-up with vegetation also improved, with PA rising to 90.59% and UA to 76.24%, indicating

fewer omission errors in suburban and peri-urban zones. Fallow land UA increased to 76.09%

while maintaining a similar PA (61.4%). Agricultural land remained highly accurate (PA

92.68%, UA 97.44%), and vegetation slightly improved in PA (66.67%) while keeping a high

UA (90.91%). Open land continued to show perfect UA (100%) and improved PA (57.89%).

Bare soil performance improved markedly (PA 50%, UA 20%). Water maintained perfect

accuracy for both metrics.

Table 5: Confusion matrix results for the classification year 2000

Class name	Open land	Agriculture	Fallow land	Vegetation	Bare soil	Ridge	Built-up with vegetation	Built-up without vegetation	Water	Total	User's Accuracy	Kappa
Open land	22	0	0	0	0	0	0	0	0	22	1	0
Agriculture	0	153	1	0	0	0	2	0	0	156	0.980769	0
Fallow land	0	13	31	1	1	0	0	0	0	46	0.673913	0
Vegetation	1	0	0	10	0	0	0	0	0	11	0.909091	0
Bare soil	2	0	0	0	1	1	2	4	0	10	0.1	0
Ridge	3	0	3	0	1	15	1	2	0	25	0.6	0
Built-up with vegetation	3	4	11	5	0	1	76	1	0	101	0.752475	0
Built-up without vegetation	11	0	5	0	1	9	12	88	0	126	0.698413	0
Water	0	0	0	0	0	0	0	0	9	9	1	0
Total	42	170	51	16	44	26	93	95	9	506	0	0
Producer's Accuracy	0.52381	0.9	0.607843	0.625	0.25	0.576923	0.817204	0.926316	1	0	0.800395	0
Kappa	0	0	0	0	0	0	0	0	0	0	0	0.749402

Table 6: Confusion matrix results for the classification year 2020

Class name	Open land	Agriculture	Fallow land	Vegetation	Bare soil	Ridge	Built-up with vegetation	Built-up without vegetation	Water	Total	User's Accuracy	Kappa
Open land	22	0	0	0	0	0	0	0	0	22	1	0
Agriculture	0	152	1	0	0	0	3	0	0	156	0.974359	0
Fallow land	0	8	35	1	0	0	1	1	0	46	0.76087	0
Vegetation	1	0	0	10	0	0	0	0	0	11	0.909091	0
Bare soil	2	0	1	0	2	1	0	0	0	10	0.2	0
Ridge	2	0	3	0	1	16	1	2	0	25	0.64	0
Built-up with vegetation	2	4	11	4	0	2	77	1	0	101	0.762376	0
Built-up without vegetation	9	0	6	0	1	10	3	97	0	126	0.769641	0
Water	0	0	0	0	0	0	0	0	9	9	1	0
Total	38	164	57	15	4	29	85	105	9	506	0	0
Producer's Accuracy	0.578947	0.926829	0.614035	0.666667	0.5	0.551724	0.905882	0.92381	1	0	0.83004	0
Kappa	0	0	0	0	0	0	0	0	0	0	0	0.786862

According to Datanovia's (n.d.) interpretation scale, the Kappa values for both years indicate "substantial agreement", underscoring the reliability of the classification outputs. Using

the classification outputs from 2000 and 2020, a change detection map was generated. Areas that underwent land cover transitions between 2000 and 2020 were categorized into nine change classes, while areas that remained unchanged were classified into nine corresponding stability classes. The accuracy assessment of the change detection map yielded and overall accuracy of 79.25% and a Kappa coefficient of 0.70.

Table 7: Accuracy Assessment results

Map Category	Overall accuracy (OA)	Kappa (k)
Classification map - 2000	80.03%	0.749
Classification map - 2020	83.04%	0.787
Change detection 2000-2020	79.25%	0.70

5. Discussion

The land use and land cover changes observed in Delhi are primarily the result of rapid urbanization, driven by significant population growth (see Figure 12), expansion of infrastructure, educational institutions, and urban development policies. Delhi's population increased sharply from 15.7 million in 2000 to 30.3 million in 2020, and it is projected to reach 43.3 million by 2035 (World Population Review, 2024). This population surge has intensified the demand for housing, employment, and public services. As a result, many open spaces have been converted into built-up areas, commercial zones, and other urban land uses.
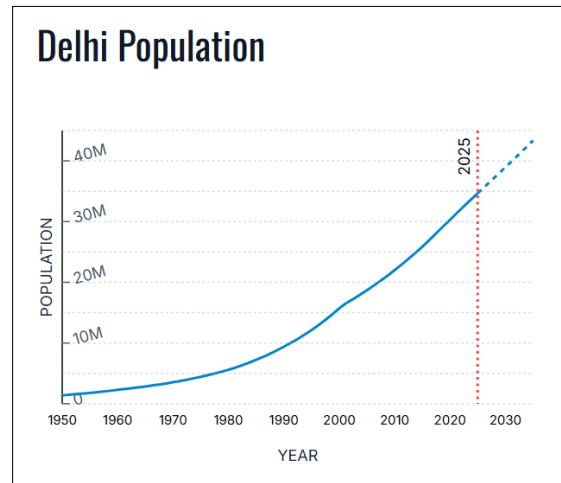
Figure 13: *The graph shows rapid increase of population in Delhi from 1950 to 2030 (Source: World Population Review, 2024)*

5.1: Change in the spatial patterns:

Urban expansion in Delhi is also closely tied to infrastructure development. For example, the construction of the Delhi Metro began in 1998, and its first line (Shahdara to Tis Hazari) opened in 2002. The network has since expanded in phases (Mohan et al., 2011). By 2020, it had become one of the world's largest urban transit systems, spanning over 300 kilometers across the National Capital Region. This increased accessibility has significantly altered land use patterns. Peripheral areas near metro lines and stations, which were once open or vegetated, have experienced substantial real estate development.

The development of built-up without vegetation is clearly visible in the eastern part of Delhi, such as Bahadurgarh, in the 2020 classification map. This area is primarily connected to the city via the Delhi Metro's Green Line and the Delhi–Rohtak corridor. Beyond the Metro, the conversion of fallow and agricultural land into built-up land is especially noticeable along newly constructed highways and expressways, such as the Peripheral Expressway and the Mumbai

Express Highway (see Figure 13). In essence, transit-oriented development (TOD) has taken root, with new apartments, malls, and office buildings emerging around metro nodes, replacing open or agricultural lands (Mohan et al., 2011).

Additionally, the construction of the Yamuna Expressway (opened in 2012) and the Eastern Peripheral Expressway (opened in 2018) has spurred development in their influence zones. This process reinforces the idea that land use planning, when integrated with transportation infrastructure, can reshape urban form. In Delhi's case, the metro has supported a more polycentric pattern of urban expansion and densification around stations, rather than concentrating all growth in the historical core.
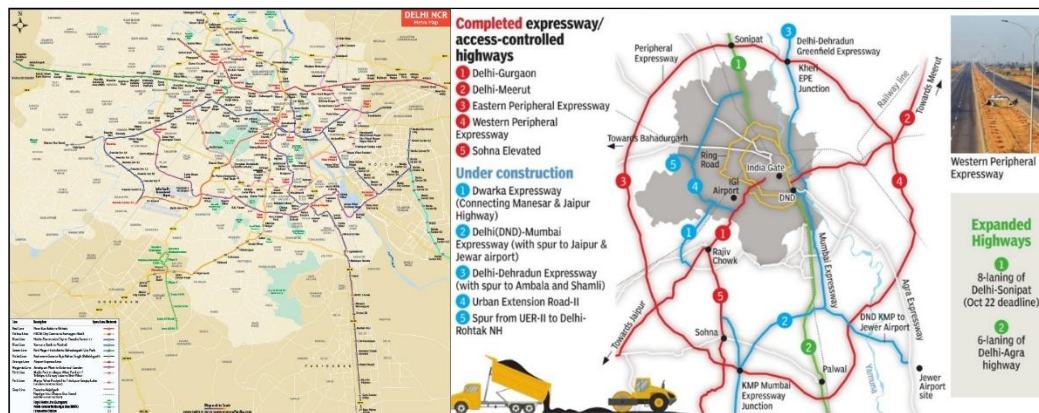
Figure 14: The images show Delhi's Metro transit network as of 2019 on the left and a web of expressways connecting Delhi with other major cities of India as of 2022 on the right (Source: Maps of India, 2019; Dabrai, R. 2024)

The Yamuna Expressway runs through rural areas southeast of Delhi, connecting Greater Noida to Agra. Large plots of farmland have been converted to new townships, industrial parks, and institutions. The Yamuna Expressway Industrial Development Authority has purchased 6,065 hectares of agricultural land to create planned urban clusters and new greenfield city along

the expressway (Property Report, 2024). This demonstrates how a single infrastructure project can trigger large scale land use change.

The Peripheral Expressway, a ring expressway that goes around the border of Delhi (see figure 13) has also enhanced connectivity in the states of Uttar Pradesh and Haryana. As a result, cities like Sonipat, Baghpat, Ghaziabad, Gurugram have emerged as the new hubs for housing colonies, warehouses and logistics parks. The influence is indirect but substantial; by diverting the traffic and economic activity just outside the city, this expressway also relieves central congestion and encourages people and businesses to locate the outskirts of the city and hence, create urban sprawl.

New policies and economic development in the 1990s and 2000s also influenced land use and land cover changes in Delhi. In the early 1990s, India's economic liberalization led to increased investment and construction, accelerating urban transformation in the following years. Several researchers have noted that the post-1991 economic reforms contributed to significant land use changes, particularly the expansion of built-up areas (Jain et al., 2016). The Delhi Master Plan 2021, introduced in the mid-2000s, strategically opened more land for urban development to accommodate housing demand. This included regularizing unauthorized colonies and converting agricultural land for urban use (Jain et al., 2016).

Other factors have also played a role in certain thematic changes, for example, the increase of the built-up with vegetation category corresponds to the rise in environmental awareness and regulatory measures. As the air pollution and the consequences of the urban heat island worsened in Delhi over the study period, government authorities and non-profit organizations emphasized green cover enhancement.

An article published by Hindustan Times (2023) cited that Delhi's green cover doubled in two decades from 10.2% in 2001 to 23.06% in 2021. Programs such as citywide tree plantation drives, initiating roadside greening programs, biodiversity parks, and regulations requiring new developments to include green spaces have contributed to increase in vegetation within the capital city (Hindustan Times, 2023). Under "Delhi Green Action Plan initiative" millions of saplings were planted every year. Hence, policy-driven environmental programs helped in reducing vegetation loss and increasing greenery within build-up environment.

In contrast to vegetation, land pressures and enforcement are contributing to the decline of Ridge Forest. The desire for good real estate in Delhi, complicated land ownership concerns, and a lack of enforcement have all contributed to the ongoing illegal construction in the Ridge areas (Agarwal, 2025). Reports document the development of farmhouses, educational institutions, and government buildings within the designated forest area.

The Ridge's scenic terrain and attractive location, and lack of developable land elsewhere are the main reasons. Besides this, urban growth demands have overridden environmental regulations. More than 38 hectares of the ridge area has been encroached at Asola village in southern Ridge. Indigenous trees, ancient rocks have been replaced by rich farmhouses (Agarwal, 2025). Finally, migration for education and employment opportunities have contributed to land use and land cover changes. This increases the demand for social and economic needs resulting in unplanned urban areas.

6. Conclusion

Land use and land cover change analysis of Delhi over the two-decade period reveals significant transformations in the city's landscape. While agricultural and open land declined, built-up areas increased substantially between 2000 and 2020. These changes highlight the capital city's rapid urbanization. The study also emphasizes the broader significance of multi-temporal LULC analysis and monitoring for environmental planning. Environmental researchers and ecologists can use the study's findings to assess ecosystem impacts such as habitat loss and the urban heat island effect, to model future scenarios, and to develop strategies for mitigating urban environmental degradation.

Regular observations of LULC changes over time are now recognized as crucial for proactive planning in India. This has even been made a national priority, with agencies like the Indian Space Research Organisation (ISRO) using multi-temporal satellite mapping to support resource management and policy-making efforts (National Remote Sensing Centre, 2024). Geospatial tools such as satellite remote sensing and Geographic Information Systems (GIS) provide detailed mapping of urbanization and land cover changes, offering reliable data to support informed decision-making. Analyses from such LULC studies are invaluable for urban planners and policymakers, helping to build sustainable development strategies and shape policies in rapidly growing megacities like Delhi (Singh, B. et al., 2022).

Finally, it is important to acknowledge the limitations of this study. It does not analyze the effects of LULC changes on the urban heat island phenomenon or associated temperature variations within the city. Another limitation is the spatial resolution of Landsat imagery (30

meters), which may overlook small-scale features. For example, narrow green belts or small water bodies may have been misclassified as other land cover types. The use of higher-resolution satellite data, such as Sentinel-2 especially for more recent years would improve classification accuracy.

References

Agarwal, P. (2025). *Delhi's ridge keeps dying: Encroachments, govt apathy undermine forests despite court orders and citizen efforts.* Times of India. https://timesofindia.indiatimes.com/city/delhi/delhis-ridge-keeps-dying-encroachments-govt-apathy-undermine-forests-despite-court-orders-and-citizen-efforts/articleshow/121664257.cms

Ahmed, M. W., Saadi, S., & Ahmed, M. (2022). Automated road extraction using reinforced road indices for Sentinel-2 data. *Array, 16*, 100257.

Asia Property Awards. (2024). *News roundup: 6,000 hectares for urban development in India, plus more news,* PropertyGuru Asia Property Awards.

Banka, R. (2023). *Capital's green cover doubled in two decades: Centre to Delhi High Court.* Hindustan Times. https://www.hindustantimes.com/cities/delhi-news/capitals-green-cover-doubled-in-two-decades-centre-to-delhi-high-court-101678733273759.html

Bikis, A., Engdaw, M., Pandey, D., & Pandey, B. K. (2025). The impact of urbanization on the land use land cover change using geographic information system and remote sensing: a case of Mizan Aman City Southwest Ethiopia. Scientific Reports, 15(1).

ChaseDay. (2024). *Delhi, India – Climate and Average Weather Year Round Insights*. ChaseDay.com. https://www.chaseday.com/delhi-india-climate-and-average-weather-year-round/

Congalton, R. G. (1991). A review of assessing the accuracy of the classification in remotely sensed data. *Remote Sensing of Environment, 37*(1), 35-46.

Dabrai, R. (2022). Web of e-ways and Highways to bring Delhi closer to key cities.

Twenty22.In. https://www.twenty22.in/2022/07/web-of-e-ways-highways-to-bring-

delhi.html

 Maps of India. (2019). *Delhi Metro Stations Map*.

https://www.mapsofindia.com/maps/delhi/delhi-metro-stations-map.html

Datanovia. (n.d.). *Kappa coefficient interpretation: Best reference*.

https://www.datanovia.com/en/blog/kappa-coefficient-interpretation/

Faizan, O. M. (2022). *Monitoring land use/land cover change and its impacts on variations of*

land surface in a rapidly urbanizing island using Google Earth Engine (GEE) – A case

study of Delhi, India. Planning Insights Research Paper.

Food and Agriculture Organization of the United Nations. (2024). *Land cover classification*

system. https://www.fao.org/4/x0596e/X0596e01e.htm

GKToday. (2022, January 25). Najafgarh jheel restoration plan. GKToday. Retrieved from

https://www.gktoday.in/najafgarh-jheel-restoration-plan/

Jain, M., Dawa, D., Mehta, R. Dimri, A.P., Pandit, M.K. (2016). Monitoring land use changes

and its drivers in Delhi, India using multi-temporal satellite data. *Modeling Earth systems*

and Environments. 2, 19.

Kafy, A., Hasib, M., Islam, M. A., Sakin, H., & Rahman, M. W. (2020) Prediction of Future

Land Surface Temperature and Its Impact on Climate Change: A Remote Sensing Based

Approach in Chattogram City. *1ˢᵗ International Student Research Conference.*

King, R., Benton, T. G., Froggatt, A., Harwatt, H., Quiggin, D., & Wellesley, L. (2023). *Chapter*

02: The state of the world's land resources - the emerging global crisis of land use: How

rising competition for land threatens international and environmental stability, and how the risks can be mitigated. The Chatham House Report.

Kottek, M., Grieser, J., Beck, C., Rudolf, B., and Rubel, F. (2006). World Map of the Koppen-Geiger climate classification updated. *Meteorologische Zeitschrift*, 15(3), 259-263.

Kshetri, T. B. (2018) NDVI, NDBI & NDWI Calculation Using Landsat 7, 8. *ResearchGate*.

Islami, F. A., Tarigan, S. D., Wahjunie, E. D., & Dasanto, B.D. (2022). Accuracy Assessment of the Land use Change Analysis Using Google Earth in Sadar Watershed Mojokerto Regency. *IOP Conference Series: Earth and Environmental Science, 950*(1), 012091.

Li, Q., Guo, H., Luo, L., Wang, X., & Yang, S. (2023). Impact Analysis of Land Use and Land cover Change on Karez in Turpan basin of China. *Remote Sensing, 15*(8), 2146.

Liu. Y., Meng, Q., Zhang, L., &Wu, C. (2022). NDBSI: A normalized difference bare soil index for remote sensing to improve bare soil mapping accuracy in urban and rural areas. *CATENA, 214*, 106265.

Mohan, M., Pathan, S. K., Narendrareddy, K., Kandya, A., Pandey, S. (2011). Dynamics of Urbanization and Its Impact on Land-Use/Land-Cover: A Case Study of Megacity Delhi. *Journal of Environmental Protection*, Vol. 2 No. 9, Doi: 10.4236/jep.2011.29147

Mountrakis, G., Im, J., Ogole, C. (2011). Support Vector Machines in Remote Sensing: A review. *ISPRS Journal of Photogrammetry and Remote Sensing, 66*(3), 247-259.

National Remote Sensing Centre. (2024). *Land use/land cover atlas of India.* Indian Space Research Organization (ISRO).

https://www.nrsc.gov.in/sites/default/files/pdf/Announcements/LULC_Atlas_NRSC.pdf

Pal, M., Mather, P. M. (2005). Support vector machines for classification of remotely sensed

    data. *Remote Sensing of Environment, 26*(5), 1007-1011.

Ram, V., Chandrashekhar Rao, R. V. R., et al., (2019). Delhi - History, Population, Map & Facts.

    Encyclopedia Britannica.

Sharma, R., & Joshi, P. K. (2016). Mapping environmental impacts of rapid urbanization in

    National Capital Region of India using remote sensing input. *Urban Climate*, 15, 70-82.

Singh, B., Venkataramanan, V. & Deshmukh, B. (2022). Monitoring of land use land cover

    dynamics and prediction of urban growth using Land change Modeler in Delhi and its

    environs, India. *Environmental Science and Pollution Research 29*, 71534-71554. Doi:

    https://doi.org/10.1007/s11356-022-20900-z

Singh, P., Chaudhuri, A. S., Verma, P., Singh, V. K., & Menna, S. R. (2022). Earth observation

    data sets in monitoring of urbanization and urban heat island of Delhi, India. *Geomatics,*

    Natural Hazards and Risk, 13(1), 1762-1779.

Singh, R., Biswakarma, P., Joshi, V., Joshi, S., Chaudhary, A. (2023). Spatiotemporal change

    analysis of land use land cover in NCT of Delhi, India using geospatial technology.

    Proceedings of the Indian National Science Academy. Part A, Physical SCIENCE. 89(1),

    189-200.

Story, M., Congalton, R. G. (1986). Accuracy Assessment: A User's Perspective. *American*

    Society for Photogrammetry & Remote Sensing, Vol. 52, No. 3.

The State of the world's land resources. (2023). Chatham House - International Affairs Think

    Tank.

World Population Review. (2024). *Delhi, India Population 2024*.

https://worldpopulationreview.com/cities/india/delhi

U. S. Geological Survey. (2024). *What are the band designations for the Landsat satellites?*

https://www.usgs.gov/faqs/what-are-band-designations-landsat-satellites

Appendix

Appendix A: Satellite Data and Metadata

Landsat ETM+ Metadata information: Image 1

Parameter	Value
Satellite	Landsat 7
Sensor	ETM+
Product ID	LE07_L2SP_146040_20000314_20200918_02_T1
Acquisition Date	March 14, 2000
Processing level	L2SP (Surface Reflectance)
Path / Row	146/040
Projection	WGS 1984 UTM ZONE 43N
Scene Center Time	05:11:24
Cloud cover	0.00% (overall and land)
Sun Azimuth / Elevation	136.34° / 49.66°
Calibration Method	LEDAPS 3.4.0
Corner Coordinates (Lat/Long)	UL: (29.83545, 76.72439), UR: (29.78240, 79.12100) LL: (27.95706, 76.69361), LR: (27.90794, 79.04765)
Corner Coordinates (UTM)	UL: (666600.000, 3301800.000), UR: (898500.000, 3301800.000) LL: (666600.000, 3093600.000), LR: (898500.000, 3093600.000)

Landsat ETM+ Metadata information: Image 2

Parameter	Value
Satellite	Landsat 7
Sensor	ETM+
Product ID	LE07_L2SP_147040_20000318_20200918_02_T1
Acquisition Date	February 18, 2000
Processing level	L2SP (Surface Reflectance)
Path / Row	147/040
Projection	WGS 1984 UTM ZONE 43N
Scene Center Time	05:17:42
Cloud cover	0.00% (overall and land)
Sun Azimuth / Elevation	142.72° / 41.24°
Calibration Method	LEDAPS 3.4.0
Corner Coordinates (Lat/Long)	UL: (29.82767, 75.15629), UR: (29.80262, 77.57722) LL: (27.92948, 75.15348), LR: (27.90631, 77.53085)
Corner Coordinates (UTM)	UL: (515100.00, 3299700.00), UR: (749100.00, 3299700.00) LL: (515100.00, 3089400.00), LR: (749100.00, 3089400.00)

Landsat OLI-TIRS Metadata information: Image 1

Parameter	Value
Satellite	Landsat 8
Sensor	OLI-TIRS
Product ID	LE08_L2SP_146040_20200210_20200823_02_T1
Acquisition Date	February 10, 2020
Processing level	L2SP (Surface Reflectance)
Path / Row	146/040
Projection	WGS 1984 UTM ZONE 43N
Scene Center Time	05:18:54
Cloud cover	2.04% (overall and land)
Sun Azimuth / Elevation	146.56° / 39.91°
Calibration Method	LaSRC 1.5.0
Corner Coordinates (Lat/Long)	UL: (29.92389, 76.79117), UR: (29.87142, 79.12776) LL: (27.84527, 76.75584), LR: (27.79709, 79.04657)
Corner Coordinates (UTM)	UL: (672900.0, 3311700.00), UR: (898800.000, 3311700.00) LL: (672900.000, 3081300.000), LR: (898800.000, 3081300.000)

Landsat OLI-TIRS Metadata information: Image 2

Parameter	Value
Satellite	Landsat 8
Sensor	OLI-TIRS
Product ID	LE08_L2SP_147040_20200217_20200823_02_T1
Acquisition Date	February 17, 2000
Processing level	L2SP (Surface Reflectance)
Path / Row	147/040
Projection	WGS 1984 UTM ZONE 43N
Scene Center Time	05:17:58
Cloud cover	0.02% (overall and land)
Sun Azimuth / Elevation	145.86° / 40.68°
Calibration Method	LaSRC 1.5.0
Corner Coordinates (Lat/Long)	UL: (29.93233, 75.20464), UR: (29.90670, 77.60436) LL: (27.83435, 75.18410), LR: (27.80952, 77.56623)
Corner Coordinates (UTM)	UL: (520800.0, 3312300.0), UR: (749700.0, 3312300.0) LL: (520800.0, 3081000.0), LR: (749700.0, 3081000.0)

Appendix B: Bands used for each spectral Index for both the years.

Normalized Difference Vegetation Index (NDVI):

NDVI Equation	$NDVI = \dfrac{NIR - RED}{NIR + RED}$
Landsat ETM+ Bands (Year - 2000)	$NDVI = \dfrac{Band\ 4 - Band\ 3}{Band\ 4 + Band\ 3}$
Landsat OLI Bands (Year - 2020)	$NDVI = \dfrac{Band\ 5 - Band\ 4}{Band\ 5 + Band\ 4}$

Normalized Difference Built-up Index (NDBI):

NDBI Equation	$NDBI = \dfrac{SWIR\ 1 - NIR}{SWIR\ 1 + NIR}$
Landsat ETM+ Bands (Year - 2000)	$NDBI = \dfrac{Band\ 5 - Band\ 4}{Band\ 5 + Band\ 4}$
Landsat OLI Bands (Year - 2020)	$NDBI = \dfrac{Band\ 6 - Band\ 5}{Band\ 6 + Band\ 5}$

Normalized Difference Water Index (NDWI):

NDWI Equation	$NDWI = \dfrac{Green - NIR}{Green + NIR}$
Landsat ETM+ Bands (Year - 2000)	$NDWI = \dfrac{Band\ 2 - Band\ 4}{Band\ 2 + Band\ 4}$
Landsat OLI Bands (Year - 2020)	$NDWI = \dfrac{Band\ 3 - Band\ 5}{Band\ 3 + Band\ 5}$

Normalized Difference Bare Soil Index (NDBSI):

NDBSI Equation	$NDBSI = \dfrac{(RED + SWIR\ 1) - (NIR + BLUE)}{(RED + SWIR\ 1) + (NIR + BLUE)}$
Landsat ETM+ Bands (Year - 2000)	$NDBSI = \dfrac{(Band\ 3 + Band\ 5) - (Band\ 4 + Band\ 1)}{(Band\ 3 + Band\ 5) + (Band\ 4 + Band\ 1)}$
Landsat OLI Bands (Year - 2020)	$NDBSI = \dfrac{(Band\ 4 + Band\ 6) - (Band\ 5 + Band\ 2)}{(Band\ 4 + Band\ 6) + (Band\ 5 + Band\ 2)}$

Road Index (RI):

RI Equation	$RI = 1 - \dfrac{3 * BLUE}{BLUE + NIR + SWIR\ 1}$
Landsat ETM+ Bands (Year - 2000)	$RI = 1 - \dfrac{3 * Band\ 1}{Band\ 1 + Band\ 4 + Band\ 5}$
Landsat OLI Bands (Year - 2020)	$RI = 1 - \dfrac{3 * Band\ 2}{Band\ 2 + Band\ 5 + Band\ 6}$